Fuel 111 (2013) 148–156

Contents lists available at SciVerse ScienceDirect

Fuel

journal homepage: www.elsevier.com/locate/fuel

Fast pyrolysis of coal, peat, and torrefied wood: Mass loss study with a drop-tube reactor, particle geometry analysis, and kinetics modeling

Henrik Tolvanen *, Lauri Kokko, Risto Raiko

Department of Chemistry and Bioengineering, Tampere University of Technology, Korkeakoulunkatu 1, 33720 Tampere, Finland

HIGHLIGHTS

- Drop-tube reactor should be coupled with optical study methods.
- Liquid nitrogen can be used to aid particle collection from drop-tube reactor.
- Particle geometry determination is necessary in biomass fast pyrolysis studies.
- Torrefied wood particle shape changes during pyrolysis with small particles.
- Density and initial volume measurements are crucial in pyrolysis modeling.

ARTICLE INFO

Article history:
Received 18 December 2012
Received in revised form 28 March 2013
Accepted 16 April 2013
Available online 4 May 2013

Keywords:
Pyrolysis
Coal
Peat
Torrefied wood
Chemical kinetics

ABSTRACT

The purpose of this study was to experimentally test and compare the fast pyrolysis behavior of torrefied wood, peat, and two types of coal. The experiments were conducted in a laboratory-scale drop-tube reactor (DTR) at a temperature range of 700–900 °C. Before pyrolysis, the sample particles were sieved with vibration sieves the opening of which was 100–125 μm. The initial size distribution of the sample particles and their diameter evolution during pyrolysis was studied by using optical techniques. According to the optical measurements particle swelling during pyrolysis occurred with the tested coal types but not with peat or torrefied wood. With torrefied wood the particle shape changed during pyrolysis from elongated to spherical. The density of the samples was measured with a mercury porosimeter. The mass loss of the sample particles during pyrolysis was modeled with two first order models: the single-step one reaction kinetics model and a model in which two reactions competed to form char and volatiles from the virgin matter. The kinetic parameters of the reactions and the diameter evolution equation coefficients were determined with both models and with all fuels. The optical measurement data from the particles was used to discretize the particle size distribution. The discretized size fractions were then used in the model calculations instead of a mono-sized single particle approach.

© 2013 Elsevier Ltd. All rights reserved.

1. Introduction

Due to coal's significant role in energy production and its harmful environmental impacts, new clean combustion technologies need to be developed if the use of coal continues. In addition to creating cleaner combustion technologies, alternative fuels must also be found and researched to replace fossil coal as an energy source. Fortunately peat and torrefied wood can be considered as fuels capable of replacing fossil coal, to some extent even in the existing power plants. However, compared to coal these fuels have different pyrolysis and combustion properties [1,2]. The differences in the volatile yield and composition between these fuels can be a major issue. The chemical kinetics, porosity, and particle shape behavior of the torrefied wood may also cause problems for example in the operation of a fuel burner in a boiler. Therefore, the usage of bio fuels in power plants and especially the modeling of these processes require more in-depth information about the fuel behavior during pyrolysis and combustion.

Torrefied wood is thermally pretreated wood that has some of the good properties of fossil coal, such as hydrophobicity. The benefit of torrefied wood as a fuel is its ability to withstand outdoor storing without losing its heating value. Compared to untreated wood it is also easier to grind [3,4]. Moreover, torrefied wood can be considered to be carbon dioxide neutral fuel. Therefore, in the world of emissions trading, many energy production companies have expressed more interest towards it. Nevertheless, the effects of torrefaction on biomass pyrolysis and combustion have

---

* Corresponding author. Tel.: +358 40 86 16 718.
E-mail address: henrik.tolvanen@tut.fi (H. Tolvanen).

0016-2361/$ - see front matter © 2013 Elsevier Ltd. All rights reserved.
http://dx.doi.org/10.1016/j.fuel.2013.04.030

yet to be studied in depth. Since the torrefied wood has been planned as a replacement fuel for fossil coal, the kinetics studies should be conducted with coal references.

Laboratory-scale testing provides useful and necessary information on solid fuel behavior during pyrolysis. This information can be used later on when designing larger power plants and burning facilities. Plenty of laboratory-scale equipment has already been developed for pyrolysis and combustion research. For example, a drop-tube reactor (DTR) can be used to simulate the temperature level, atmosphere, and heating rate of fluidized bed combustion and pulverized fuel firing; processes that are characteristic for power plants. Among others [5] have noticed that pyrolysis kinetics change substantially when the heating rate varies. Therefore, new advanced experimental setups should be developed in order to provide insight on the behavior of both fossil fuels and different types of biomass under conditions that resemble those of industrial-scale plants. As a result of the high heating rate a DTR can be seen as a more appropriate tool for studying solid fuel pyrolysis than, for example, a thermogravimeter. Experimental and modeling studies have also been conducted in fluidized bed environment. Papadikis combined multiphase flows with discrete particle tracking by incorporating an external user defined function in FLUENT and modeled biomass particle fast pyrolysis in a bubbling fluidized bed reactor [6,7]. Bruchmüller's et al. [8] work investigated fast pyrolysis in a fluidized bed reactor from a particle-scale perspective taking also into account mixing, segregation and entrainment of the biomass. However, the measurement setup used in this work enables the investigation of the sample particles' actual size and shape before and after pyrolysis. This information is important if different particle geometries are taken into account in modeling. Among others Lu has showed in his work [9] that biomass particle shape has a great impact on the conversion rate.

Several types of models have already been presented in the literature and employed to describe the pyrolysis process of solid fuel particles [6]. However, despite the ability of these models to accurately describe the phenomena related to pyrolysis, strongly simplified kinetics models have also been used successfully [10,11]. If the results of these kinetic analyses are to be used in computational fluid dynamics (CFD) calculations, it is clear that complex models are more time demanding. Therefore, simplified models should be favored if their accuracy is close to the complex ones. Instead of complicated models the emphasis should be on defining accurate initial parameters for the modeling calculations. Thus, it is important to note that the initial parameters of pyrolysis modeling, such as fuel density and diameter distribution, have a tremendous effect on the calculated kinetic parameters. The novelty value of this work lies in the complementary usage of optical techniques and mercury porosimeter in the sample particle shape and mass determination as well as in the liquid nitrogen drop-tube reactor collecting system.

2. Materials and methods

2.1. Fuel composition and sample preparation

In this study, four different solid fuels were tested: two types of coal, peat, and torrefied wood. The two coal types formed a reference to which the peat and torrefied wood samples could be then compared. The ultimate and proximate analyses of the fuels were conducted by Enas Co. and the results are presented in Table 1.

It can be seen from Table 1 that there is only minor difference in the composition of the two coal samples. The largest fractional difference was in their sulfur content.

The torrefied wood sample material was received in the form of pellets. From the torrefied wood raw material 90% was softwood, and the rest was hardwood. The stem wood raw material was first chipped and then torrefied. The torrefaction was done at 250 °C in a continuous operated reactor. The residence time of the chips in the reactor was approximately 0.5 h. The mass yield of the torrefaction process was 89.6% from the original weight. The torrefied wood was then pelletized with a ring matrix pelletizer.

The density of the samples used in the experiments was measured with a Micromeritics Poresizer 9320 mercury porosimeter in the Department of Civil Engineering at Tampere University of Technology. The density measurements were conducted with the same sample particle size as used in the pyrolysis tests. The measured intrinsic (skeletal) density of the sample fuel materials and the evaluated apparent density values of the ground sample particles are presented in Table 2. The intrinsic density of the samples was calculated according to the mercury intrusion volume when all the pores greater than 6 nm were filled. The apparent density was evaluated with a mercury intrusion threshold of 26 μm. The threshold value was chosen according to the evaluated resolution of the already defined particle projection surface area. In the mercury intrusion volume curve as a function of average pore diameter, the 26 μm value appeared to be the point where mercury had filled most of the gaps between the particles and started intruding inside them. In this way, the evaluated particle apparent density and the particle volume based on image analysis could be used to calculate the mass of the particles.

The coal 1 sample batches treated at 700 °C and 850 °C were sieved with ring sieves sized 100–125 μm and the batch at 900 °C later on with 112–125 μm sieves. The coal 2 sample batches were all sieved with 100–125 μm sieves. The peat sample batches were sieved with 112–125 μm sieves but there were two different batches, one for 700 °C and 850 °C temperatures and one for 900 °C. Finally, the torrefied wood sample batches were all sieved with 112–125 μm sieves. Before sieving the samples were dried in an oven at 105 °C for 24 h and the crushed with a Retsch ZM 200 centrifugal mill. The sieving was conducted several times for a single sample with a vibration sieve in order to obtain a narrow size fraction. Between the sample preparation and the measurements, the sample was kept in an exicator with silica gel to remove the moisture from it. Therefore, in the modeling phase the particles were assumed to be dry when they entered the reactor.

2.2. Drop-tube reactor

The DTR system used in this study was designed by the first author. The design was based on the previous versions constructed at the Tampere University of Technology. The reactor consisted of three different modular parts: a feeding probe, a reactor part, and a new improved fuel collecting system. The reactor itself was an austenitic stainless steel tube with an inside diameter of 26.7 mm, and with a temperature resistance up to 1300 °C. The reactor was covered with 2–7 $\Omega\,m^{-1}$ resistance wire sets, which formed eight separately adjustable heating elements. The heating elements were insulated with an approximately 7 cm thick layer of kaowool. The heating zone length of the reactor was 65 cm and it was followed by 2.5 cm of unheated zone. The DTR and the auxiliary equipment are presented in Fig. 1.

Furthermore, windows for optical measurement purposes were built into the reactor, and they were placed at the lower end of the heating zone. The center point of the windows was 53.5 cm below the start of the heating zone. The windows were placed as low as possible in the reactor to enable particle velocity measurements with longer residence times. As already mentioned, after the heating zone end, there was a 2.5 cm section of unheated reactor tube, which was left between the resistance wires and the collecting system to prevent excess heating of the collecting vessel.

Table 1
The results of the ultimate and proximate analyses for the tested fuels.

Analysis	Peat	Coal 1	Coal 2	Torrefied wood	Unit
Ash content (815 °C)	7.1	13.7	15.4	0.2	dry wt.%
Volatile matter	65.4	34.5	31.4	81.9	dry wt.%
Sulfur	0.14	0.33	1.37	<0.02	dry wt.%
Carbon	52.6	67.8	64.8	53.2	dry wt.%
Hydrogen	5.5	4.6	4.5	6	dry wt.%
Nitrogen	1.24	2.04	2.07	<0.2	dry wt.%
Oxygen (calculated)	33.42	11.53	11.86	40.38	dry wt.%
Calorimetric heating value	20.96	28.05	28.2	21.07	MJ/kg
Lower heating value	19.76	27.06	27.24	19.77	MJ/kg

Table 2
The measured intrinsic densities of the samples and the evaluated apparent densities of the sample particles.

Sample	Intrinsic density (kg/m^3)	Apparent density (kg/m^3)
Peat	1245	459.7
Coal 1	1412	1050
Coal 2	1353	1251
Torrefied wood	1208	931.0

The main function of the feeding probe was to carry the particles to a wanted level inside the reactor and maintain them at a low enough temperature before entering the heating zone. The particles were inserted to the feeding probe from a feeding silo. Around the particle feeding tube was a water cooling jacket that kept the inside temperature of the probe at less than 80 °C. This ensured that the pyrolysis process of the sample particles started only after they entered the reactor itself. The temperature of the reactor wall was constantly measured from eight points and the gas temperature inside the reactor was measured before every run. From this data, average temperature profiles were first generated for the reactor wall and gas temperatures. These temperature profiles were then used in the energy balance equation as the gas and wall temperatures. The volume flow of nitrogen inside the reactor at 0 °C was $1.585\,\mathrm{l\,mol^{-1}}$, which corresponded with the average gas velocities of $0.1735\,\mathrm{m\,s^{-1}}$, $0.200\,\mathrm{m\,s^{-1}}$, and $0.209\,\mathrm{m\,s^{-1}}$ at furnace temperatures of 700 °C, 850 °C and 900 °C respectively. The calculated Reynolds number for the reactor gas flow was well in the laminar zone in each of the aforementioned conditions.

The collecting system was designed to quench and cool down the particles very rapidly. This was achieved by floating the collecting vessel on liquid nitrogen. The vessel was placed near the reactor exit and while the gases erupted out from the edges, the collecting vessel acted as an impactor and collected the particles. The evaporating nitrogen kept the atmosphere totally inert. This collecting system improved the accuracy of the measurements significantly. As the drop-tube reactor was constructed the mass loss measurement accuracy was tested with coal and biomass particles. A simple way of testing the system accuracy was pyrolyzing sample particles in the reactor and increasing the reactor length after the final volatile yield was reached. If the yield stayed the same with greater particle falling lengths it meant that no particles were lost to the walls. Tests were also made in cold state to see whether all the particles that were fed were collected. The collecting system made it possible to collect all the particles that were dropped to the reactor, which in turn made the mass loss measurements simple and accurate.

2.3. High-speed camera

A high-speed camera was used for taking photographs of the particle stream inside the reactor through the measuring windows. The recorded pictures were then analyzed with a computer program in order to determine the velocity of the particles. The camera was an AVT Marlin 145-B2 with a 1380 × 1090 resolution and with a black and white CCD-cell. The camera was placed in front of the measurement windows, and the background led-light was placed to the opposite side of the reactor. The falling particles generated a double shadow to the image because of the pulsating LED-light located on the opposite side of the reactor. Based on the distance of the shadows and the time delay between the two pulses, the analysis program could determine the velocity of the particles. However, the images had to be scaled before the measurements.

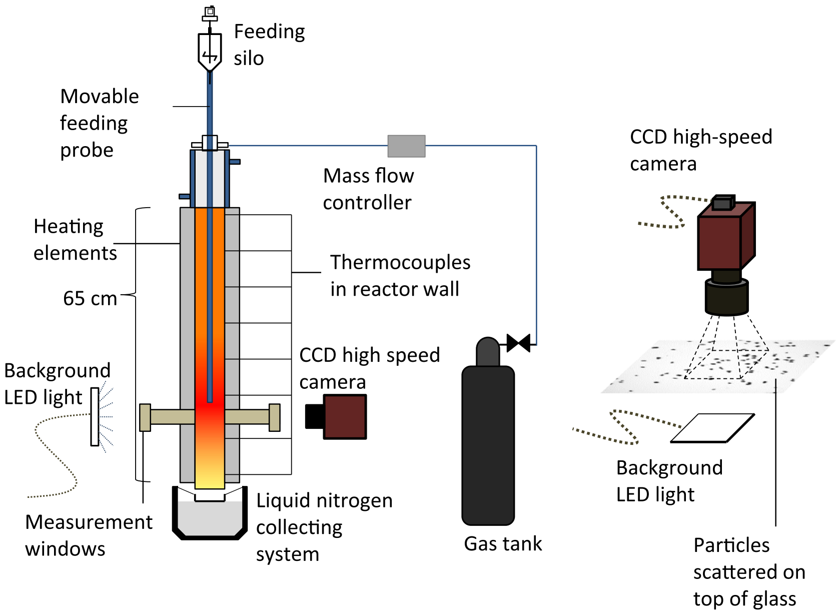

Fig. 1. A description of the DTR on the left and the diameter measurement system on the right.

Before recording, the camera was focused by running some particles through the reactor and adjusting the camera distance and aperture accordingly. Using a high-speed camera eliminated the need to calculate the particle residence time in the reactor with the particle motion equation. Instead, the velocity was first measured from several stages in the reactor by moving the position of the particle feeding probe. Based on these measurements, velocity profiles were generated for each cases and the residence time could then be integrated from them. An example of the velocity measurements and the generated fits can be seen in Fig. 2.

Fig. 2 shows that the velocity profile of the particles was not even, since there was a rather large increase in the gas velocity after the probe tip. However, it was visually observed that this acceleration in the speed did not spread the particle stream. The acceleration in the speed resulted from the geometry inside the reactor.

2.4. Determining particle diameter

The diameter of the particles was determined in a separate stage after the reactor treatment. First, the particles were scattered on a glass plate that was luminated from below. Here, the CCD camera was used to take pictures of the particle projections. On top of the plate the particles were easier to focus than while falling inside the reactor. The images were analyzed with a program developed by PhD Markus Honkanen from Tampere University of Technology. The analysis program recognized the particle projection outlines and calculated the pixel based projection area. In each diameter measurement round, altogether over thousand particles were detected from the images. The mass mean diameter of the sample particles could be determined by first calculating their volume and assuming they all had the same density. Fig. 3 illustrates the particle projection outline recognition of the crushed and sieved sample particles.

Fig. 3 shows remarkably that the vibration sieving process produced mostly homogeneously sized and shaped spherical particles with the coal samples. Unfortunately, this was not the case for peat and especially for torrefied wood. The torrefied wood particles were highly elongated. This can most likely be explained by the fibrous structure of wood. If the projection area of the torrefied wood and peat particles would have been considered as projection of a sphere, it would have highly exaggerated the initial particle mass. Therefore, the elongated particles were considered to be the shape of cylinders.

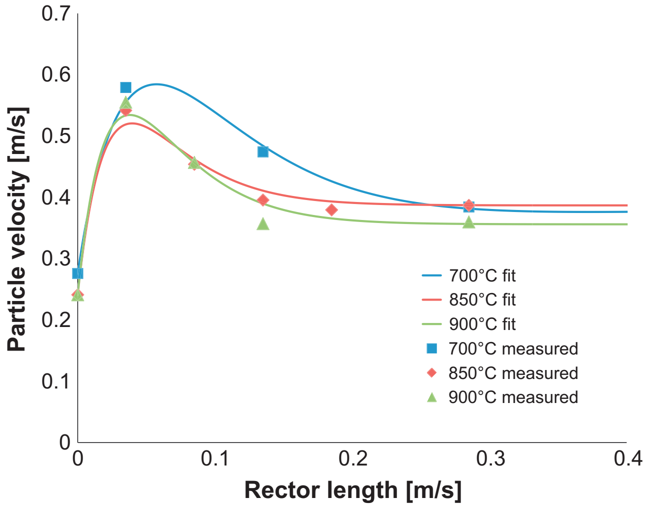

Fig. 2. The measured velocity values and the generated fits for the peat sample particles. The zero point in the horizontal axis represents the probe tip.

The analysis program made an ellipse fit to describe the particle dimensions and outlines. The dimensions of the ellipse could be used to estimate the sphericity of the particle. A set value of 1.5 was used for the individual particle ellipse maximum to minimum length ratio to distinguish between spheres and cylinders. If the particle had a ratio below 1.5 when calculating its volume, it was assumed as sphere when calculating its volume and if equal or over 1.5, the shape was assumed to be cylindrical. The cylinder thickness was calculated by dividing the projection area with the maximum ellipse length of the particle. The maximum ellipse length was used instead of the minimum, since the ellipse fit seemed to exaggerate the minimum length for the elongated particles. With this approach the particle volume could be calculated more accurately. The presented mass mean diameters were calculated backwards from the volume. For easier comparability, the presented diameters are those of a sphere with an equal volume. Therefore, the diameter values presented in this study describe more the volume change than the actual shape change of the particles. The heat transfer coefficient for all particles was calculated according to the spherical diameter. The particle size data in turn was used to calculate the volume distribution of the particles. Finally, the volume distribution was discretized for the modeling stage.

3. Modeling

3.1. Modeling the mass loss chemical kinetics

The mass loss chemical kinetics of the samples was modeled with two simple models: a one reaction and a two-competing reactions model. The one reaction model was chosen as it is commonly used in CFD calculations. The two competing reactions model was chosen to serve the need to preform solid fuel pyrolysis CFD calculations with a wider particle diameter distribution. The kinetic parameters related to the models were calculated with an optimization routine that minimized the difference between the measured values and the model prediction.

In the one reaction model there was a predetermined amount of volatiles in the particle that was released through one global reaction. The one reaction mass loss rate was expressed as follows:

$$-\frac{dm_p}{dt} = k(VM_0 - X_{DAF})m_0(1 - Ash) \tag{1}$$

The term m_p is the mass of the particle (kg) at given time, m_0 is the initial mass of the particle (kg), t is the time (s), k is the reaction rate coefficient (s^{-1}), and X_{DAF} is the conversion stage (–) of the particle that indicates the amount of fractional mass loss in dry ash-free (DAF) form. The term VM_0 describes the initial fractional amount of volatiles in the particle and it has to be determined at each temperature. It was also used in DAF form. The term Ash is the fractional amount of ash in the particle based on its initial dry mass. The reaction rate coefficient was of the Arrhenius form:

$$k = Ae^{\left(-\frac{E_a}{R_u T_p}\right)} \tag{2}$$

where A is the pre-exponential factor of the reaction rate coefficient (s^{-1}), E_a is the exponential factor of the reaction rate coefficient ($J\,mol^{-1}$), R_u is the universal gas constant ($J\,mol^{-1}\,K^{-1}$), and T_p is the particle temperature (K). In the two reaction model both reactions competed to form volatiles and char. Therefore, no predetermined amount of volatiles at a certain temperature was needed in the calculations. This was an advantage compared to the one reaction model. The mass loss rates of the two competing reactions were expressed as follows:

$$-\frac{dm_p}{dt} = \frac{dm_{volatiles}}{dt} = k_{volatiles}(1 - X_{char} - X_{volatiles})m_0(1 - Ash) \tag{3}$$

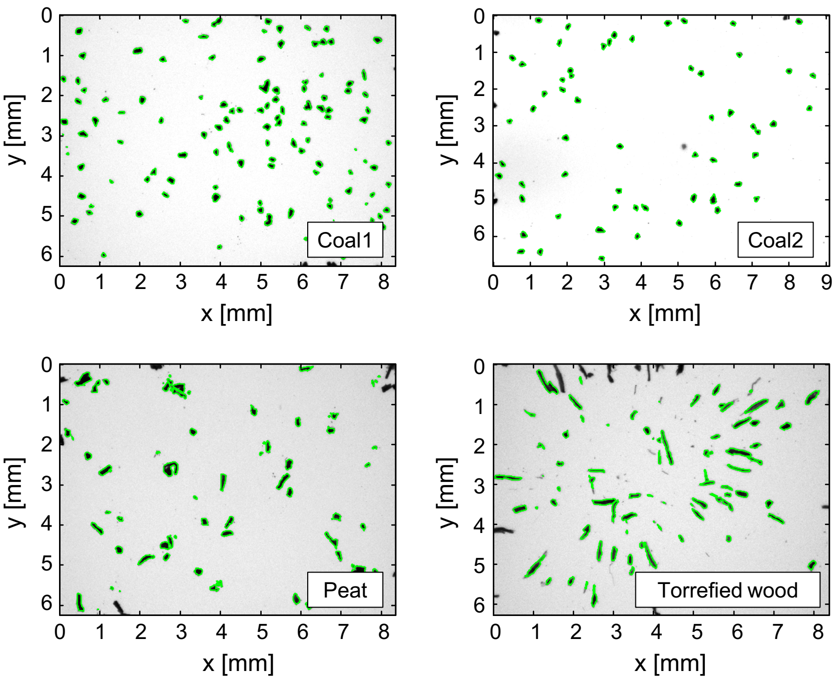

Fig. 3. The particle projection outline recognition with the diameter analysis program from the sieved sample parties before pyrolysis. The green line around the particles illustrates the outline recognition.

$$\frac{dm_{char}}{dt} = k_{char}(1 - X_{char} - X_{volatiles})m_0(1 - Ash) \tag{4}$$

where $m_{volatiles}$ is the amount of volatiles released (kg), m_{char} is the amount of virgin matter converted to char (kg), k_{char} and $k_{volatiles}$ describe the reaction rate coefficients for the char and volatiles formation reactions (s^{-1}) respectively. The term X_{char} is the fractional amount of DAF virgin material converted to char (–), and $X_{volatiles}$ is the fractional amount of DAF virgin material converted to volatiles (–). Both reactions stopped when all the virgin material had transformed into char or volatiles.

3.2. Modeling the particle diameter evolution

The diameter evolution for peat and torrefied wood particles during pyrolysis was modeled with the following equation:

$$d = d_0(1 - X)^{\beta} \tag{5}$$

where d is the diameter of the particle (m) at a given time and d_0 is the particle initial diameter (m). If the term β is 0, the particle diameter remains constant and its density decreases during pyrolysis. If β is negative it means that the particle size increases as the virgin matter conversion to volatiles advances. The maximum value of 1/3 for β describes a situation where the density remains constant and the diameter decreases. This equation was suitable to describe the shrinkage of the peat and torrefied wood particles during pyrolysis. Nevertheless, with the coal samples an additional term was introduced to the diameter evolution equation to describe the swelling that occurred especially at the highest temperature of 900 °C, where also the mass loss rate was the highest. Therefore, the swelling term was set to be dependent on the mass loss rate as follows:

$$d = d_0\left((1 - X)^{\beta} + \frac{dX}{dt}\varphi\right) \tag{6}$$

The coefficient φ described the magnitude of the swelling. In both Eqs. (5) and (6) the conversion stage X was in the dry form in the range of $0\ldots X_{char}(1 - Ash)$.

3.3. Particle energy balance

The following equation describes the energy balance of the pyrolyzing particle in the DTR:

$$m_p c_p \frac{dT_p}{dt} = \theta A h_c(T_{gas} - T_p) + A_p \varepsilon\sigma\left(T_{wall}^4 - T_p^4\right) + h_{pyr}\frac{dm}{dt} \tag{7}$$

where m_p is the mass of the particle (kg), c_p is the specific heat capacity of the particle (J kg^{-1} K^{-1}), T_p is the temperature of the particle (K), t is the time (s), the term θ describes the effect of the Stefan flow on the particle convective heat transfer (–), A_p is the surface area of a spherical particle (m^2) with a diameter of d_p, h_c is the heat transfer coefficient (W m^{-2} K^{-1}), T_{gas} is the measured gas temperature in the rector (K), ε is the emissivity of the particle (–), σ is the Stefan–Boltzmann constant (W m^{-2} K^{-4}), T_{wall} is the measured wall temperature of the reactor (K), and h_{pyr} is the pyrolysis enthalpy (J kg^{-1}). The term on the left hand side describes the energy stored in the particle. The first term on the right hand side describes the heat convection to the particle from the surrounding gas, the second term describes the radiative heat transfer between the wall and the particle, and the third term describes the internal heat generation or consumption due to the chemical reactions taking place during pyrolysis. The heat transfer coefficient was calculated with the Ranz and Marshall [12] correlation. The heat capacity of the DAF material in the particle was modeled according to Merrick [13]:

$$c_{p,DAF} = \frac{R_u}{M_{ave}}\left[\left(\frac{T_{E1}}{T_p}\right)^2 \frac{e^{T_{E1}/T_p}}{(e^{T_{E1}/T_p} - 1)^2} + 2\left(\frac{T_{E2}}{T_p}\right)^2 \frac{e^{T_{E2}/T_p}}{(e^{T_{E2}/T_p} - 1)^2}\right] \tag{8}$$

where M_{ave} is the average molar mass of the elements in the DAF matter (kg^{-1} mol) and T_{E1} and T_{E2} are the Einstein temperatures (K). The Einstein temperatures selected for the heat capacity determining were 380 K and 1800 K. The heat capacity for the ash was calculated as follows:

$$c_{ash} = 754 + 0.586T_p \tag{9}$$

The Stefan flow term θ in the convection part of the energy balance equation was used as presented in [14]. The following correlation applies to the Reynolds numbers up to 400 [14]:

$$\theta = e^{(-0.6B)} \tag{10}$$

where B is related to the total gas release from a particle (–):

$$B = \frac{c_{vol}}{2\pi d_p k_g}\left(\frac{dm_p}{dt}\right) \tag{11}$$

Above c_{vol} is the heat capacity of the volatiles (J kg^{-1} K^{-1}) and k_g is the conductivity of the gas (W m^{-1} K^{-1}). As a result of the unknown content of the volatile gases, in this research article their heat capacity was assumed to be the same as that of carbon dioxide.

The emissivity of the particle in the radiation part was set to be 0.9 as proposed by [15]. Due to the small size of the particles the Biot number was small enough for the assumption that they were thermally thin. Studies suggest that biomass particle diameter of about 250 μm is the upper limit for a uniform temperature ($Bi < 1$) [16]. Also Papadikis et al. [7] showed in his calculations that with a convective heat transfer coefficient of approximately one third in comparison to the one in this study and with 500 μm particles the internal temperature gradient is negligible. Therefore, the internal heat transfer of the particles was not taken into consideration in the calculations in this study. The pyrolysis enthalpy for all the reactions in the two models was set to be 120 kJ kg^{-1}(endothermic). The particle temperature was solved from the energy balance equation by first linearizing the radiation term according to [17] and then discretizing the time dependance of the variables.

3.4. Discretizing the particle size distribution

The particle size distribution was calculated for the initial samples according to the analyzed diameter data. The distribution was discretized into ten equal-sized volume fractions. After this, the volume mean diameter of each fraction was calculated. The volume mean diameters obtained were then used as initial diameters in the model calculations. Thus, the model results were volume-averaged. The averaging was done as follows:

$$F_{avg} = \sum_{n=1}^{10} F_n v_n \tag{12}$$

where F_{avg} is the averaged variable (X, T_p, c_p, or d_p), F_n is a variable ($X_n, T_{p,n}, c_{p,n}$, or $d_{p,n}$) related to the nth volume fraction, and $v_n = 0.1$ is the volume fraction. Fig. 4 shows an example of the minimum, the maximum, and the volume-averaged mass loss values calculated with both models.

Fig. 4 shows that with the two competing reactions model the final mass loss levels of the volume fractions were not the same. This results from the different heating rates. With smaller particles the heating rate was higher and the temperature in the particles increased more rapidly. The higher temperature in the small particles favored the reaction that formed volatiles. With the one reaction model, the fixed amount of volatiles resulted in even final volatile matter amounts between the volume fractions. Due to the small particle size their terminal velocity was small compared to the gas velocity. Thus, the velocity of the particles in the reactor was assumed to be the same regardless of the particle size. Therefore, there was no difference in the residence times between different volume fractions.

3.5. Objective function and the optimization routine

A MATLAB-based objective function was written to determine the kinetic parameters of the selected reactions. The objective function minimized the square error between the mass loss and diameter model predictions and the measured values. The optimization routine used MATLAB's fminsearch function. The errors from the mass loss and diameter comparisons were summed in such a way that the mass loss error was emphasized ten fold compared to the diameter error. This was done because of the greater variance in the diameter measurements and because the mass loss was of greater importance when determining the chemical kinetic parameters. A lower limit of 20 kJ mol^{-1}was set for the exponential factors of the reaction rate coefficients.

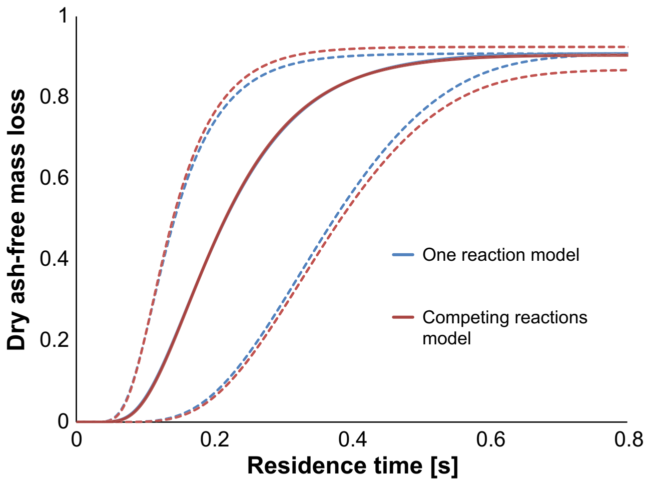

Fig. 4. The dry ash-free mass loss as a function of residence time for torrefied wood. The dashed lines are the maximum and minimum diameter groups and the middle one is the average value of all 10 volume fractions.

4. Results and discussion

4.1. Experimental and modeling results

The behavior of peat and torrefied wood during pyrolysis differed greatly from that of the two types of coal both in terms of diameter evolution and the rate of mass loss. The absolute reaction rates (kg s^{-1}) of the torrefied wood were much higher than those of the coals even though their densities were similar. It was also noted that during pyrolysis swelling of the particles occurred with the coals but not with peat or torrefied wood. The volume fractions of the samples that were determined based on the images from the initial samples are presented in Fig. 5.

The volumes of the particles for Fig. 5 were calculated according to the procedure described in the Section 2.4. The coal 1 histogram in Fig. 5 shows the effect of switching the lower sieve from 100 μm to 112 μm. For both coal types the diameter distribution is reasonable in relation to the sieve sizes. The peat and torrefied wood histograms, on the other hand show higher volume concentrations on significantly larger diameters than the sieve sizes. It can be explained with elongated particles and the spherical equivalent diameter calculation. This shows that if the initial mass of the particles is calculated purely based on the sieve opening sizes and an assumption of particle sphericity, the possibility of a major error increases.

The measured mass loss in DAF form and the diameter values along with the mass loss fit from the two-competing reactions model and the diameter evolution equation fit are presented in Figs. 6–9. The model values were calculated up to 40 cm reactor length. The one reaction model results are not presented in the figures. They were similar with the competing reactions model. However, the error function value was always greater in all the one reaction model results.

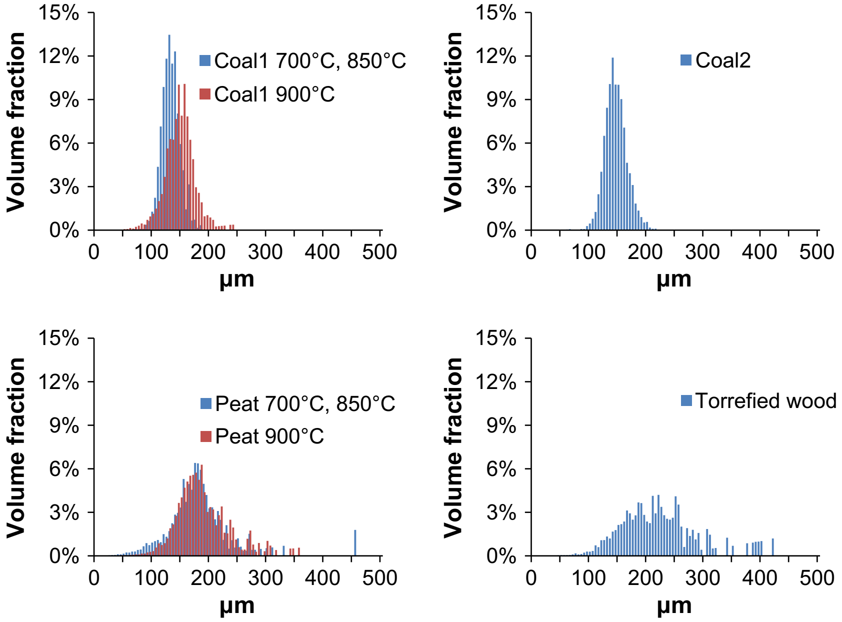

Fig. 5. The initial sample volume fractions based on the image analysis. The temperatures in the coal 1 and peat sample legends refer to the reactor temperatures at which the batches were used.

For easier comparability the measured diameter values in Figs. 7 and 9 were calculated based on particle volumes and presented as diameters of spheres with equal volumes. Fig. 6 shows that the competing-reactions model was able to describe the measured mass loss fairly accurately with coal 1. With peat the model did not meet the measured values as well at the two highest temperatures quite so well. In this study, torrefied wood had the highest mass loss rate during pyrolysis. With Peat, at 850 °C and 900 °C all the measured values were already close to the final volatile matter. It also seemed that no distinct isoconversion level was reached with peat, and the measured mass loss values slowly increased towards the end of the measurements. This can be explained, for example by slower reactions taking place or merely by a slight error in the mass loss measurements. These phenomena most likely reduced the accuracy of the determined kinetic parameters for the peat sample. However, in Fig. 8 the measured mass loss values matched the model prediction as closely as with coal 1.

The char yield for torrefied wood in Fig. 8 was approximately 5% in DAF form at 900 °C. A very similar value for woody biomass particles sized 0.35 mm char yield in a DTR was reported in [18]. The conversion profile of the torrefied wood particles is very similar to that reported by Umeki et al. [19] for same sized lignocellulosic biomass particles in an entrained flow reactor. The residence time differences in reaching the maximum conversion level might be due to different temperature profiles in the reactors. Lehto [11] reported a DAF volatile yield of approximately 88% for Finnish milled peat tested in a DTR at 800 °C with a same particle size fraction as used in this work. The volatile matter amount of peat differs from the one measured in this work most likely due to the different decomposition stages of the peat samples.

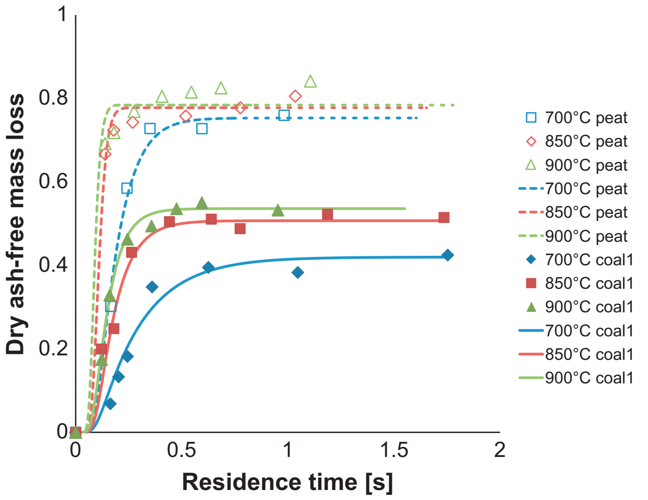

Fig. 6. The dry ash-free mass loss as a function of residence time for peat and coal 1. The dots represent the measured values and the continuous and the dashed lines the model.

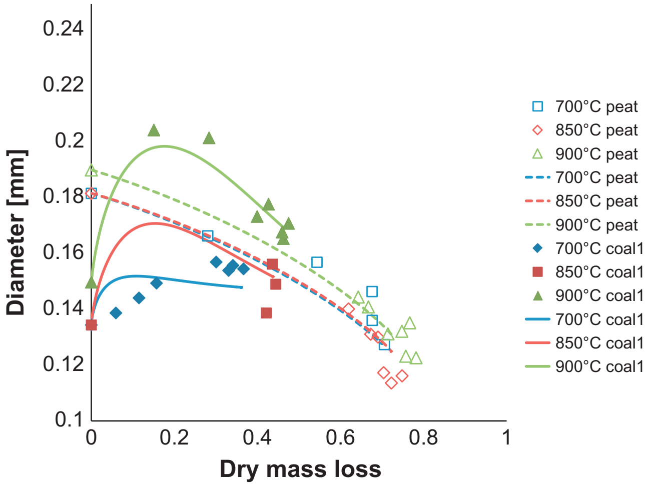

Fig. 7. The particle diameter evolution as a function of dry mass loss for peat and coal 1. The dots represent the measured values and the continuous and the dashed lines the model.

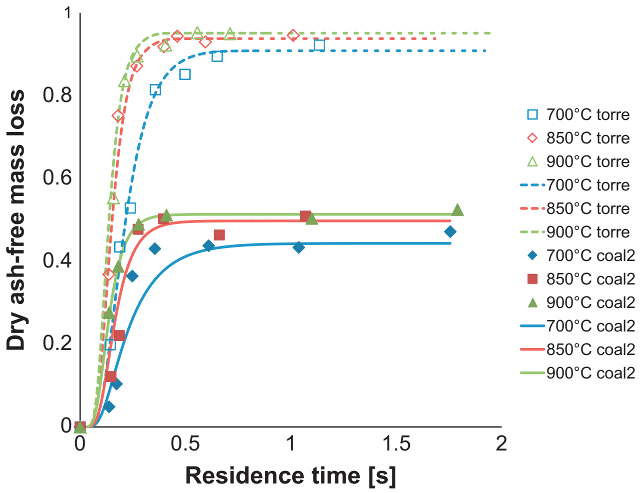

Fig. 8. The dry ash-free mass loss as a function of residence time for torrefied wood and coal 2. The dots represent the measured values, and the continuous and the dashed lines the model.

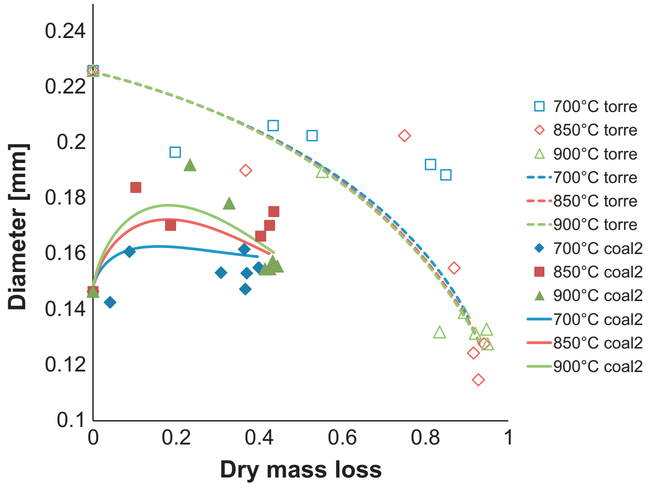

Fig. 9. The particle diameter evolution as a function of dry mass loss for torrefied wood and coal 2. The dots represent the measured values, and the continuous and the dashed lines the model.

Table 3
The one reaction model kinetic parameter and the diameter evolution equation coefficients.

Sample	(1/s)	(kJ/mol)	(–)	(–)
Peat	577,800	87.46	0.2806	–
Coal 1	1230	44.78	−0.2019	0.08049
Coal 2	1352	42.42	−0.1530	0.04265
Torrefied wood	19,250	56.78	0.1989	–

Table 4
The final volatile matter amount for the samples at each temperature measured with the DTR.

Sample	At 700 °C	At 850 °C	At 900 °C
Peat	0.6860	0.7249	0.7686
Coal 1	0.3459	0.4393	0.4656
Coal 2	0.3750	0.4209	0.4343
Torrefied wood	0.9067	0.9358	0.9489

Table 5
The two-competing-reactions kinetic parameters and the diameter evolution equation coefficients.

Sample	(1/s)	(kJ/mol)	(1/s)	(kJ/mol)	(–)	(–)
Peat	942,600	102.7	17,010,000	116.7	0.2930	–
Coal 1	276.2	37.20	5260	62.97	−0.2031	0.07606
Coal 2	420.0	38.23	1472	48.92	−0.1460	0.04323
Torrefied wood	10.95	20.00	34,550	61.44	0.2170	–

The peat and coal 1 sample batches treated at 900 °C were different than those treated at 700 °C and 850 °C. Therefore, the initial volume mean diameter of the particles was somewhat different between them. This shows clearly in Fig. 7. Figs. 7 and 9 show that both coals swoll during the pyrolysis. However, the swelling did not occur with peat or torrefied wood.

Even though 112–125 μm sieves were used the sample particle initial diameters were much higher in each case as can be seen from Figs. 7 and 9. The deviation is most likely caused by the elongation of the particles, especially with the peat and torrefied wood samples. As the particles were scattered on top of the glass after pyrolysis they were on their side and thus created the largest possible projection from themselves. Even with the rather spherical coal particles this resulted in measured initial volume mean diameters that were slightly higher than the sieve sizes. The large initial diameter of the particles could also have been a result of too small resolution when imaging the particles. However, when the camera was zoomed closer, the results were more or less the same. The main goal in the imaging stage was to have as many particles in the picture with adequate resolution as possible.

The images that were taken for the diameter analysis also revealed the changes in the sample particle shapes during pyrolysis. First of all, the coal particles seemed to remain spherical. The peat sample particles also seemed to maintain their elongated shape.

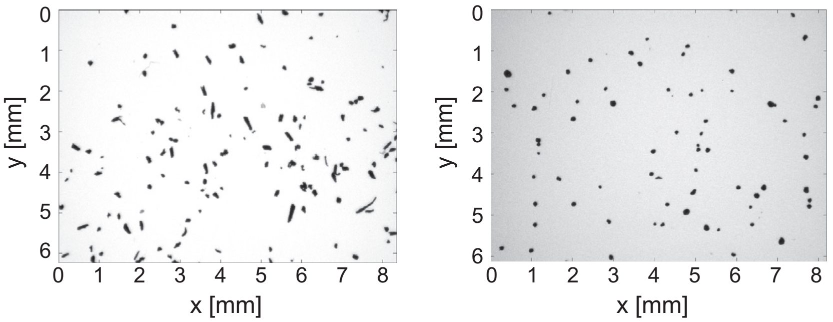

Fig. 10. The shape of the peat and torrefied wood sample particles at the end of pyrolysis. Both samples were treated at 850 °C for 40 cm in the reactor. Peat is on the left and torrefied wood on the right.

The torrefied wood sample particles, on the other hand looked like droplets at the end of pyrolysis. This can be seen in Fig. 10.

The same observation could be made from the ellipse fit maximum and minimum length based aspect ratios. With peat the aspect ratio remained close to the initial value, but the ratio for torrefied wood decreased so that in the end it was close to one. The reason for this behavior could be the differences in the chemical composition of the peat and torrefied wood samples. For instance, some of the components in torrefied wood may have liquid intermediates. Biagini et al. [20] reported slight decrease in the aspect ratio of woody biomass particles. The particles in Biagini's study were sized >0.3 mm. However, the change in the aspect ratio was not as high as observed in this study. Peat has a higher content of ligning compared to torrefied wood, which in turn has a higher amount of cellulose and hemicellulose in it. The high amount of lignin in peat could result as more durable shape structure of small particles during pyrolysis.

4.2. Fitted parameters

The chemical kinetic parameters and the diameter evolution equation coefficients were calculated with the MATLAB-based optimization algorithm by comparing the model prediction to the measurements conducted. The parameters related to the one reaction model are presented in Table 3.

The final volatile matter amounts for the sample fuels at all the measured pyrolysis temperatures are presented in Table 4.

The volatile matter amounts in Table 4 are in dry form. They were determined from the measured mass loss values by calculating the average of the mass loss after it had reached a clear plateau. The chemical kinetic parameters and the diameter evolution equation coefficients related to the two-competing-reactions model are presented in Table 5.

The diameter evolution equation exponent β was negative and the swelling magnitude term φ was above zero for the coal samples in both Tables 3 and 5. This indicates that the diameter of the coal particles increased due to the swelling.

5. Conclusion

The constructed DTR measurement system proved to be a fast and accurate tool for conducting mass loss and diameter evolution measurements with coal and biomass particles. Especially the new liquid nitrogen quench collecting system and the particle falling velocity measurement with the high-speed camera eliminated a large number of uncertainties from the mass loss measurements and from determining the particle residence times. The measurements indicated that the from all the four tested fuels, torrefied wood had the greatest volatile matter amount. With all four fuels the final volatile yield in the DTR was larger than the proximate analysis had indicated. This shows again how important it is to use a suitable heating rate in chemical kinetic studies in relation to industrial applications. The optical study of the sample particles demonstrated that the sample material had a clear influence on the shape of the particles. With fibrous material the outcome of the preprocessing is most likely to be elongated or cylindrical particles. Therefore, if the initial mass of the particles is calculated purely based on the sieve sizes and on the assumption of spherical particle geometry, there is a possibility of great error. The image analysis also showed that with the torrefied wood sample the shape of the particles seemed to change from elongated to spherical during pyrolysis. The volume calculation based on particle projection coupled with the mercury-porosimeter-based density measurement offered means to improve the accuracy of the particle initial mass calculation. The two chosen pyrolysis models were able to describe the mass loss behavior of the fuels fairly well. Furthermore, the diameter evolution equations provided means to predict the volume change of the sample particles.

Acknowledgments

The authors gratefully acknowledge the financial support of Metso Co., Fortum Co., UPM-Kymmene Co., Pohjolan Voima Co., and Helen Co., for this study.

References

[1] Jones J, Bridgeman T, Darvell L, Gudka B, Saddawi A, Williams A. Combustion properties of torrefied willow compared with bituminous coals. Fuel Process Technol 2012;101(0):1–9. ISSN 0378-3820.

[2] Steenari B-M, Lindqvist O. Fly ash characteristics in co-combustion of wood with coal, oil or peat. Fuel 1999;78(4):479–88. ISSN 0016-2361.

[3] Kokko L, Tolvanen H, Hämäläinen K, Raiko R. Comparing the energy required for fine grinding torrefied and fast heat treated pine. Biomass Bioenergy 2012;42(0):219–23. ISSN 0961-9534.

[4] Repellin V, Govin A, Rolland M, Guyonnet R. Energy requirement for fine grinding of torrefied wood. Biomass Bioenergy 2010;34(7):923–30. ISSN 0961-9534.

[5] Wiktorsson L-P, Wanzl W. Kinetic parameters for coal pyrolysis at low and high heating rates: a comparison of data from different laboratory equipment. Fuel 2000;79(6):701–16. ISSN 0016-2361.

[6] Papadikis K, Gu S, Bridgwater A, Gerhauser H. Application of CFD to model fast pyrolysis of biomass. Fuel Process Technol 2009;90(4):504–12. ISSN 0378-3820.

[7] Papadikis K, Gu S, Bridgwater A. CFD modelling of the fast pyrolysis of biomass in fluidised bed reactors. Part B: Heat, momentum and mass transport in bubbling fluidised beds. Chem Eng Sci 2009;64(5):1036–45. ISSN 0009-2509.

[8] Bruchmüller J, van Wachem BGM, Gu S, Luo KH, Brown RC. Modeling the thermochemical degradation of biomass inside a fast pyrolysis fluidized bed reactor. AIChE J 2012;58(10):3030–42. ISSN 1547-5905.

[9] Lu H, Ip E, Scott J, Foster P, Vickers M, Baxter LL. Effects of particle shape and size on devolatilization of biomass particle. Fuel 2010;89(5):1156–68. ISSN 0016-2361.

[10] Blondeau J, Jeanmart H. Biomass pyrolysis in pulverized-fuel boilers: derivation of apparent kinetic parameters for inclusion in CFD codes. Proc Combust Inst 2011;33(2):1787–94. ISSN 1540-7489.

[11] Lehto J. Determination of kinetic parameters for Finnish milled peat using drop tube reactor and optical measurement techniques. Fuel 2007;86:1656–63. ISSN 0016-2361.

[12] Ranz JWE, Marshall WR. Evaporation from drops, part II. Chem Eng Prog 1952;48:173–80.

[13] Merrick D. Mathematical models of the thermal decomposition of coal: 2. Specific heats and heats of reaction. Fuel 1983;62(5):540–6. ISSN 0016-2361.

[14] Solomon PR, Serio MA, Suuberg EM. Coal pyrolysis: experiments, kinetic rates, and mechanisms. Prog Energy Combust Sci 1992;18:133–220.

[15] Solomon PR, Hamblen DG, Serio MA, Yu Z-Z, Charpenay S. A characterization method and model for predicting coal conversion behaviour. Fuel 1993;72(4):469–88. ISSN 0016-2361.

[16] Yang YB, Sharifi VN, Swithenbank J, Ma L, Darvell LI, Jones JM, et al. Combustion of a single particle of biomass. Energy Fuels 2008;22(1):306–16.

[17] Mills AF. Basic heat and mass transfer. Prentice Hall; 1999.

[18] Septien S, Valin S, Peyrot M, Spindler B, Salvador S. Influence of steam on gasification of millimetric wood particles in a drop tube reactor: experiments and modelling. Fuel 2013;103(0):1080–9. ISSN 0016-2361.

[19] Umeki K, Kirtania K, Chen L, Bhattacharya S. Fuel particle conversion of pulverized biomass during pyrolysis in an entrained flow reactor. Ind Eng Chem Res 2012;51(43):13973–9.

[20] Biagini E, Narducci P, Tognotti L. Size and structural characterization of lignin-cellulosic fuels after the rapid devolatilization. Fuel 2008;87(2):177–86. ISSN 0016-2361.